International Journal of Thermal Sciences 88 (2015) 201–214

Contents lists available at ScienceDirect

International Journal of Thermal Sciences

journal homepage: www.elsevier.com/locate/ijts

Entropy generation analysis for laminar thermal augmentation with conical strip inserts in horizontal circular tubes

Yonghua You [a], Aiwu Fan [b,*], Yuming Liang [b], Shiping Jin [b], Wei Liu [b], Fangqin Dai [a]

[a] State Key Laboratory of Refractory and Metallurgy, Wuhan University of Science and Technology, Wuhan 430081, China
[b] School of Energy and Power Engineering, Huazhong University of Science and Technology, Wuhan 430074, China

ARTICLE INFO

Article history:
Received 13 December 2013
Received in revised form
27 August 2014
Accepted 8 October 2014
Available online 3 November 2014

Keywords:
Entropy generation analysis
Thermal augmentation
Thermo-hydraulic performance
Laminar flow
Conical strip inserts
Numerical simulation

ABSTRACT

Our previous investigations demonstrated that conical strip inserts have good thermo-hydraulic performances based on evaluation criteria of the First Law of Thermodynamics. The present work is dedicated to further analyze the performances of these inserts from a viewpoint of entropy generation. Effects of alignment method and geometrical parameters on entropy generations of laminar heat transfer in the tubular flow are investigated. Local entropy generations are presented for discussion. Results show that entropy generation rates caused by non-staggered strips are about 81.1% that of staggered alignment, while the heat transfer rates and PECs of the former are about 33.8% and 13.5% larger than the latter counterparts, respectively. Moreover, the entropy generation rate (and thus irreversible loss) caused by heat transfer process overwhelms the counterpart by viscous flow. The total entropy generation number of enhanced tube, ranging between 0.0657 and 0.0975, is most sensitive to geometry angle with a maximum averaged relative variation of 32.2%. Its variation trend with Re is concave with a pit at Re = ~600. In brief, non-staggered inserts with a larger geometry angle and smaller strip-wall gap and pitch, facilitate a better thermo-hydraulic performance at Re = ~600 from the viewpoint of exergy loss reduction.

1. Introduction

For energy saving and cost reduction, heat transfer enhancement in heat exchangers has been extensively studied for several decades. Numerous thermal augmentation techniques have been developed and applied in various industrial fields to make the heat transfer process more efficient [1–8].

Enhancing the heat transfer rate on the tube side is always highlighted for the improvement of overall performance of heat exchangers. A variety of high efficient tubes, for example, spirally corrugated tube [9], helically rib-roughened tube [10], and micro-fin tube [11], have been developed for better performances on the tube side. Meanwhile, many kinds of tube inserts have been investigated for the tube-side enhancement. The twisted tapes are one type of frequently adopted inserts with good performance [12,13], because they generate spiral flow in tubes, which promotes the blending of bulk fluid and disturbs thermal boundary layer as well. However, the increment of flow resistance induced by a conventional twisted tape is relatively larger. To crack the nut, many developments and modifications have been presented, to name a few, segmented twisted tapes [14,15], broken twisted tapes [16], and center-cleared twisted tapes [17], etc. Wire coil is another type of tube inserts for heat transfer enhancement. It could induce spiral flow near the wall and block the development of viscous sublayer. Thus, the thermal augmentation is efficient in the turbulent regime, while the flow resistance is relatively smaller [18,19].

Usually, the heat transfer enhancement is accompanied by an increment in the flow resistance or required pumping power. In order to comprehensively evaluate the overall thermo-hydraulic performance, both the heat transfer rate and flow resistance should be taken into consideration. Up to now, a variety of performance evaluation criteria (PEC) have been proposed [20], to list a few, $[(Nu/Nu_0)/(f/f_0)]^{1/3}$, $(K/K_0)/(\Delta p/\Delta p_0)$ and $(h/h_0)/[(W/A)/(W/A)_0]^{1/3}$ are some frequently adopted ones, in which the subscript 0 stands for the values before being enhanced.

It is noted that the above-mentioned PECs make use of combined parameters based on the First Law of Thermodynamics, and no considerations are given to the irreversible losses of the energy quality or exergy. As is well known that heat transfer is driven by

* Corresponding author. School of Energy and Power Engineering, Huazhong University of Science and Technology, 1037 Luoyu Road, Wuhan 430074, China. Tel.: +86 27 87542618; fax: +86 27 87540724.
E-mail addresses: faw@hust.edu.cn, hust_yyh@163.com (A. Fan).

http://dx.doi.org/10.1016/j.ijthermalsci.2014.10.003
1290-0729/

Nomenclature

b	strip pitch, m
c_V	specific heat of constant volume, J/(kg K)
D	tube diameter, m
f	friction factor
g	gravitational acceleration, m/s^2
Gr	Grashof number
h	convection heat transfer coefficient, W/(m^2 K)
K	overall heat transfer coefficient, W/(m^2 K)
L	length, m
Nu	Nusselt number
N_s	entropy generation number
p	pressure, Pa
Δp	pressure loss, Pa
q_T	heat flux, W/m^2
q_V	volumetric flow rate, m^3/s
Re	Reynolds number
s	entropy, J/(kg K)
S_g^c	local entropy generation rate, W/(m^3 K)
S_g^t	tube entropy generation rate, W/K
T	temperature, K
u	velocity, m/s
W	pumping power, W
x, y, z	coordinate axis, m
ρ	density, kg/m^3
μ	dynamic viscosity, N s/m^2
λ	thermal conductivity, W/(m K)
α	slant angle, °
β	geometry angle, °
δ	strip-wall gap, m
γ	mean pressure gradient, Pa/m
α_V	volume expansion coefficient, 1/K

Subscripts

f	fluid
i, j	tensor
in	inlet
m	mean
out	outlet
w	tube wall

temperature difference, and heat amount keeps constant during the transfer process. However, according to the Second Law of Thermodynamics, the quality of thermal energy is degraded and some amount of exergy is dissipated. Meanwhile, extra entropy will be generated. Therefore, for a heat transfer process where the exploitation of exergy is highlighted, the analysis method based on exergy loss should be taken instead to minimize the entropy generation for an optimal design [21–23]. Although the minimal entropy generation principle was proposed several decades ago, many researchers still employ this principle in their studies on thermal augmentation [24–31]. Sahin [24] computed the dimensionless entropy generation to determine the optimum duct shape with constant heat flux and circular geometry was found to be the best. Moreover, he revealed that the viscous entropy generation becomes dominant under the condition of low heat flux [25]. Ko and Ting [26] and Ko [27] made use of the minimal entropy generation principle to optimize laminar forced convection in a rectangular curved duct with longitudinal ribs. They compared various rib arrangements and discovered that mounting a single rib on the heated wall could reduce the entropy generation most effectively.

Fan et al. recently developed a new insert with segmental conical strips for heat transfer enhancement, and demonstrated these inserts had good thermo-hydraulic performances based on the First Law of Thermodynamics in both turbulent and laminar flow regimes [32,33]. The current work is dedicated to further investigate the laminar thermal augmentation with conical strip inserts from the viewpoint of minimal entropy generation, including comparing thermo-hydraulic performances of enhanced tubes with staggered and non-staggered strip inserts, and examining the effects of geometrical parameters of strip inserts on the irreversible losses of convective heat transfer.

2. Numerical model and computational scheme

2.1. Physical model

Fig. 1(a) and (b) schematically shows the horizontal circular tubes fitted with non-staggered and staggered conical strip inserts, respectively. The inner diameters, D, of both tubes are 0.02 m. The dimension of conical strip is characterized by a geometry angle, β (=30°, 45°, 60° and 90°). The slant angle α (=30°, 40° and 50°) refers to the angle between the conical strip and the central rod. The strip-wall gap (δ) and strip pitch (b) are normalized by tube diameter D, with δ/D taking the values of 0.10, 0.15, 0.20 and 0.25, while b/D taking the values of 1.5, 2.25 and 3.0.

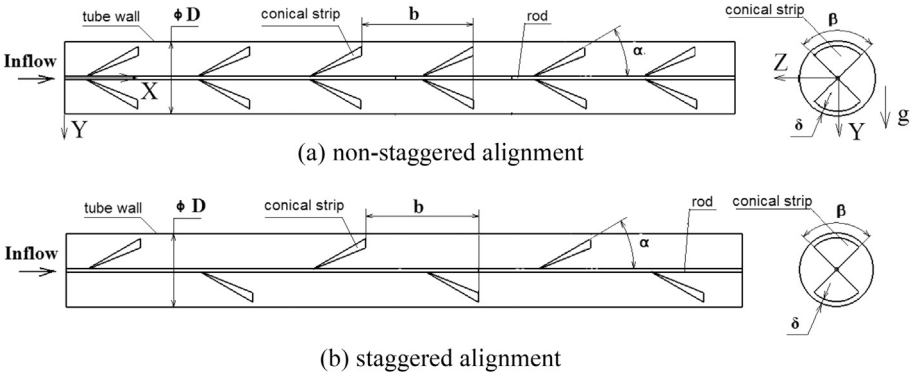

Fig. 1. Schematics of enhanced tubes with conical strip inserts. (a) Non-staggered alignment; (b) staggered alignment.

2.2. Governing equations

The present flow is assumed to be in the laminar regime. Air is selected as the working fluid, which is treated as a Newtonian, incompressible fluid. Because the averaged temperature differences between the bulk fluid and tube wall are not that large (<30 K) in the current investigation, the physical properties of working fluid are considered to be constant [34], and the buoyancy effect is ignored, which is to be checked in Section 2.4. Moreover, it is assumed that the deformation of conical strip inserts is not considered. In addition, the assumption of quasi-steady convection heat transfer is adopted to decrease the computation load [35,36]. The conservation equations of continuity, momentum and energy for the convective heat transfer of working fluid are presented in the tensor form as following:

Continuity equation:

$$\frac{\partial(\rho u_j)}{\partial x_j} = 0 \tag{1}$$

Momentum equation:

$$\frac{\partial(\rho u_i u_j)}{\partial x_j} = -\frac{\partial p}{\partial x_i} + \frac{\partial}{\partial x_j}\left(\mu\left(\frac{\partial u_i}{\partial x_j} + \frac{\partial u_j}{\partial x_i}\right)\right) \tag{2}$$

Energy equation:

$$\frac{\partial(\rho c_V T u_j)}{\partial x_j} = \frac{\partial}{\partial x_j}\left(\lambda\left(\frac{\partial T}{\partial x_j}\right)\right) + \mu\frac{\partial u_i}{\partial x_j}\left(\frac{\partial u_i}{\partial x_j} + \frac{\partial u_j}{\partial x_i}\right) \tag{3}$$

where T and p stand for fluid temperature and pressure, respectively; u is the fluid velocity; ρ and c_V are fluid density and specific heat at constant volume, respectively; and λ and μ are thermal conductivity and dynamic viscosity, respectively.

The conical strips, made of stainless steel, don't contact with the tube wall (see Fig. 1). However, they could impact the temperature field of working fluid through their internal heat conduction and convection heat transfer with air, which favors the heat transfer enhancement and the reduction of entropy generation. The strips have a thickness of 1 mm, whose temperature fields are determined by Eq. (4), together with the conjugate heat transfer between the fluid and strips.

$$\frac{\partial}{\partial x_j}\left(\lambda_s\left(\frac{\partial T}{\partial x_j}\right)\right) = 0 \tag{4}$$

where λ_s refers to the heat conductivity of strips.

Since the strips are arranged with constant pitch, to minimize the computation load and for the convenience of comparison, the convection heat transfer is assumed to be fully developed, thus the periodical model can be adopted, i.e., only one cycle of tube is modeled in the present investigation. In the construction of periodic model, a transform is conducted by introducing an intermediate variable of pressure [37], i.e.,

$$\widehat{p} = p(x,y,z) + \gamma\cdot(x - L_c) \tag{5}$$

where γ and x refer to the averaged longitudinal pressure gradient and the longitudinal coordinate, while L_c equals to the length of one cycle. As for the case of non-staggered alignment, L_c takes strip pitch (b), thus $\gamma = [p(x, y, z) - p(x + b, y, z)]/b$.

It is clear that $\widehat{p}$ varies periodically in the fully developed region, and the momentum equation can be re-written based on the intermediate variable $\widehat{p}$. The real pressure can be obtained by Eq. (5) after the convergence of iteration.

2.3. Computation region, mesh and boundary conditions

In the current numerical model, one cycle of the enhanced tube is adopted as the computation domain, and periodic boundary condition is applied to the inlet and outlet of the domain [37]. Meanwhile, due to the symmetric geometries of the circular tubes, only half of and a quarter of them are chosen for the staggered and non-staggered alignments in our computation, respectively. The software Gambit 2.4 is adopted for the geometrical modeling and meshing, and both tetrahedral mesh and hexahedral mesh are adopted. In order to resolve the variations of entropy generations near the walls, mesh refinement is conducted in these regions. The computation domains and grid systems, for enhanced tubes with conical strips of staggered and non-staggered alignments, are shown in Fig. 2(a) and (b), respectively, which both consist of a fluid zone (air) and a solid zone (strip).

Momentum boundaries of no slip and no penetration are set for all solid walls. The tube wall has a thermal boundary condition of uniform heat flux, while the boundary of thermally coupled wall is set for the interface between fluid and solid. In order to obtain an approximately constant temperature difference between tube wall and working fluid, the value of heat flux on tube wall is proportional to the Re number, and the slope is approximately the same as that of Nu number.

As for the periodic boundary, the mass flow rate needs to be given for bulk flow, then the CFD software computes the fluid velocity and temperature fields at the inlet by iteration [37]. In the current investigation, the specified mass flow rates insure that the tubular flow is always in the laminar regime.

2.4. Computational scheme and validation

The commercial CFD software, Fluent 12.0 [38], is used to solve these governing equations. The conservation equations and boundary conditions are discretized by finite volume formulation. The momentum and energy terms are treated with the second-order upwind scheme, while the pressure term takes the standard scheme. The gradients on the faces are evaluated with the Node-Based method, i.e., taking the arithmetic average of the nodal values on the face. The double-precision segregated solver is adopted for the computation, and pressure and velocity are coupled with the 'SIMPLE' algorithm. The convergence criteria are set as: relative residual of 1E−5 for both continuity and momentum and 1E−8 for energy.

The present numerical methods are validated by computing a smooth tube, a full-length enhanced tube and a one-cycle enhanced tube in our previous paper [33], where the computed Nu number and f factor of smooth tube have relative deviations within ±3% against the theoretical counterparts. The check of grid independence is conducted for staggered and non-staggered alignments, respectively. For the non-staggered alignment, three grid systems (about 80,000, 125,000 and 210,000 cells) are computed, and the moderate grid is adopted for the final computation since the relative deviations of Nu and f between the last two systems are only 1.5% and 3.2%, respectively. The staggered alignment uses a similar grid system to that of non-staggered one, and the grid system of 500,000 cells is ultimately adopted by comparing three grid systems (about 320,000, 500,000 and 800,000 cells).

The effect of buoyancy is evaluated with the combined criterion (Gr/Re^2) in the current investigation. Since uniform heat flux is set on the tube wall, the temperature field of tubular flow is symmetrical, and tube radius is adopted as the characteristic dimension of Gr number ($=\rho^2 g D^3 \alpha_V (T_{w,m} - T_{f,m})/8\mu^2$). Therefore, in the present investigation, the Gr of tubular flow is smaller than 4000, and the

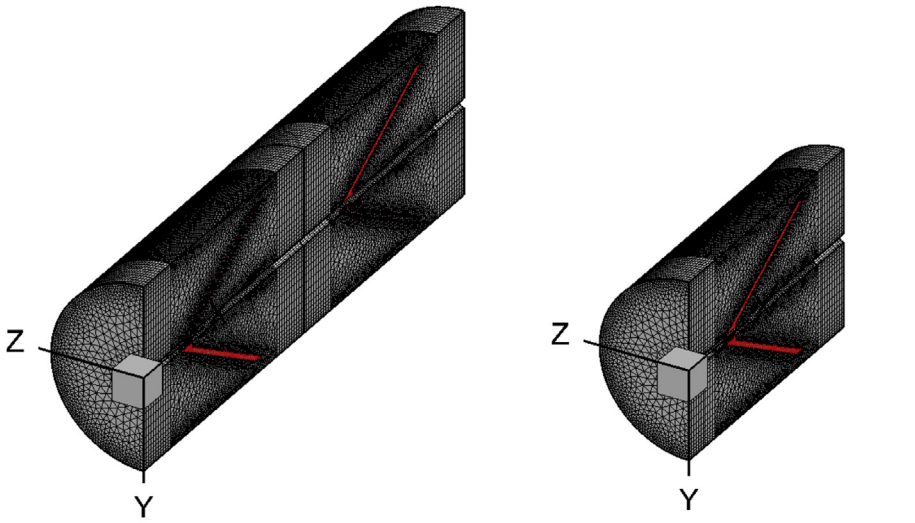

Fig. 2. Computation domains and meshes for enhanced tubes with strips of staggered and non-staggered alignments, red represents the strips. (a) Staggered alignment; (b) non-staggered alignment (For interpretation of the references to color in this figure legend, the reader is referred to the web version of this article.).

value of Gr/Re^2 is less than 0.045 at Re = 300–1800, which indicates the tubular flow is always in the forced laminar regime [34].

In addition, the numerical computation on a full-section horizontal tube of one periodic length is conducted to examine the effect of buoyancy force in the above Re ranges for both staggered and non-staggered alignments, where the density of air is set to be temperature dependent. The relative deviations of Nu and f of non-staggered alignment from the counterparts of fluid with constant density are less than 3% at Re = 300–1800, while the counterparts of staggered alignments are less than 4.5%. Therefore, in the present investigation, the Re is set in the range between 300 and 1800, and thus the buoyancy can be neglected in the computation.

3. Calculation methods of thermo-hydraulic performances

Despite that entropy generation based on the Second Law of Thermodynamics is highlighted in the current study, we still pay close attention to heat transfer rate and flow resistance, because they not only reflect the direct gain and cost of thermal augmentation, but also influence the entropy generations greatly. The calculation methods of thermo-hydraulic performances are listed as following.

3.1. Heat transfer rate, friction factor and overall performance evaluation criterion (PEC) based on the First Law of Thermodynamics

Heat transfer rate is expressed by the Nusselt number, Nu, which is calculated as

$$\mathrm{Nu} = \frac{q_{\mathrm{T,w}}}{T_{\mathrm{w,m}} - T_{\mathrm{f,m}}} \cdot \frac{D}{\lambda} \tag{6}$$

where D, λ and $q_{\mathrm{T,w}}$ stand for the tube diameter, air thermal conductivity and heat flux of tube wall, respectively. $T_{\mathrm{w,m}}$ stands for the area-weighted mean temperature of tube wall, while $T_{\mathrm{f,m}}$ represents the arithmetic mean value of the averaged temperatures of working fluid at the inlet and outlet, respectively, i.e., $T_{\mathrm{f,m}} = (T_{\mathrm{in,m}} + T_{\mathrm{out,m}})/2$. The calculation of the averaged temperature of inlet fluid is presented by Eq. (7), and the averaged fluid temperature at the outlet can be obtained with the same way.

$$T_{\mathrm{in,m}} = \iint_{\Sigma} \rho u_x T_{\mathrm{f}} \,\mathrm{d}y\mathrm{d}z \Big/ \iint_{\Sigma} \rho u_x \,\mathrm{d}y\mathrm{d}z \tag{7}$$

Here u_x and T_{f} refer to the local axial velocity and temperature of fluid, respectively. Σ represents the section of the inlet.

The friction factor, f, is calculated as

$$f = \frac{2\gamma D}{\rho u_{\mathrm{m},x}^2} \tag{8}$$

where $u_{\mathrm{m},x}$ stands for the mean axial velocity of cross section, while D and γ represent the diameter and mean axial pressure gradient, respectively.

The overall thermo-hydraulic performance evaluation criterion based on the First Law of Thermodynamics is presented by Eq. (9) [20,33], where the Nu_0 and f_0 represent the Nu number and f factor of smooth tube at the same Re condition.

$$\mathrm{PEC} = \left(\frac{\mathrm{Nu}/\mathrm{Nu}_0}{(f/f_0)^{1/3}} \right) \tag{9}$$

3.2. Entropy generation rate and entropy generation number

Taking an arbitrary cell from the computation domain for consideration, the total entropy generation rate of stable convection heat transfer can be calculated by the following entropy balance equation [39].

$$S_{\mathrm{g}}^{\mathrm{c}} = -\frac{1}{T}\nabla\cdot(\lambda\nabla T) + \frac{\lambda|\nabla T|^2}{T^2} + \rho u\cdot\nabla s \tag{10}$$

where u and T stand for the velocity vector and temperature of working fluid, while s and $S_{\mathrm{g}}^{\mathrm{c}}$ represent entropy and local entropy generation rate, respectively.

Combining Eqs. (3) and (10), together with the First Law of Thermodynamics (i.e., $c_V \mathrm{d}T = T\,\mathrm{d}s - p\,\mathrm{d}V$), one can obtain the local

entropy generation rate of incompressible fluid, as shown in Eq. (11) [25,26].

$$S_g^c = S_{g,\Delta T}^c + S_{g,\Delta p}^c = \frac{\lambda}{T^2}|\nabla T|^2 + \frac{\mu}{T}\frac{\partial u_i}{\partial x_j}\left(\frac{\partial u_i}{\partial x_j}+\frac{\partial u_j}{\partial x_i}\right) \tag{11}$$

where the first term on the right hand side stands for the entropy generation arising from heat conduction, i.e., $S_{g,\Delta T}^c = (\lambda/T^2)|\nabla T|^2$, while the second term represents the entropy generation caused by viscous flow, i.e., $S_{g,\Delta p}^c = (\mu/T)\,(\partial u_i/\partial x_j)\,[(\partial u_i/\partial x_j)+(\partial u_j/\partial x_i)]$.

The above derivation is conducted for the local entropy generation. If we apply the entropy balance principle to a whole tube, the total entropy generation rate of the tube can be obtained, as shown in Eq. (12) [39].

$$S_g^t = S_{g,\Delta t}^t + S_{g,\Delta p}^t = \left(\rho q_V c_p \ln\left(\frac{T_{out,m}}{T_{in,m}}\right) - \frac{q_{T,w}\pi DL}{T_{w,m}} - \frac{q_V\cdot\Delta p}{T_{f,m}}\right) + \frac{q_V\cdot\Delta p}{T_{f,m}} \tag{12}$$

where q_V is the volumetric flow rate; $T_{in,m}$ and $T_{out,m}$ stand for the fluid temperatures of inlet and outlet, respectively, while $T_{f,m}$ refers to the averaged value of fluid temperatures at the inlet and outlet. The last term on the right hand side of Eq. (12), represents the whole entropy generation rate resulting from viscous flow, i.e., $S_{g,\Delta p}^t = (q_V\cdot\Delta p)/T_{f,m}$, while the three terms in the bracket stand for the entropy generation rate due to heat transfer, i.e., $S_{g,\Delta T}^t = \rho q_V c_p \ln(T_{out,m}/T_{in,m}) - (q_{T,w}\pi DL/T_{w,m}) - [(q_V\cdot\Delta p)/T_{f,m}]$.

For the conveniences of the comparisons of irreversible losses between enhanced tubes with different cycle length, the tubes of same length (i.e., 9*D*) are computed for the entropy generation rates. In the computation, it is assumed that each cycle has the same averaged convection heat transfer coefficient (or Nu number) and pressure loss.

It is seen from Eq. (12) that the entropy generation rate depends on the heat flux and temperature of tube wall. For easier comparisons between different cases, various dimensionless entropy generation numbers have been presented and widely applied [40–42]. In the current investigation, the total entropy generation number normalized by the entropy flow through the tube wall is adopted [42], as shown in Eq. (13).

$$N_s = \frac{T_{w,m}\left(S_{g,\Delta T} + nS_{g,\Delta p}\right)}{q_{T,w}\pi DL} \tag{13}$$

where *L* is the calculated tube length, equal to 9*D*. The factor *n* is for the conversion efficiency from exergy of thermal energy to mechanical work. The value of *n* ranges from 5.5 to 7.0 [42], and here a typical value of 6.0 is adopted.

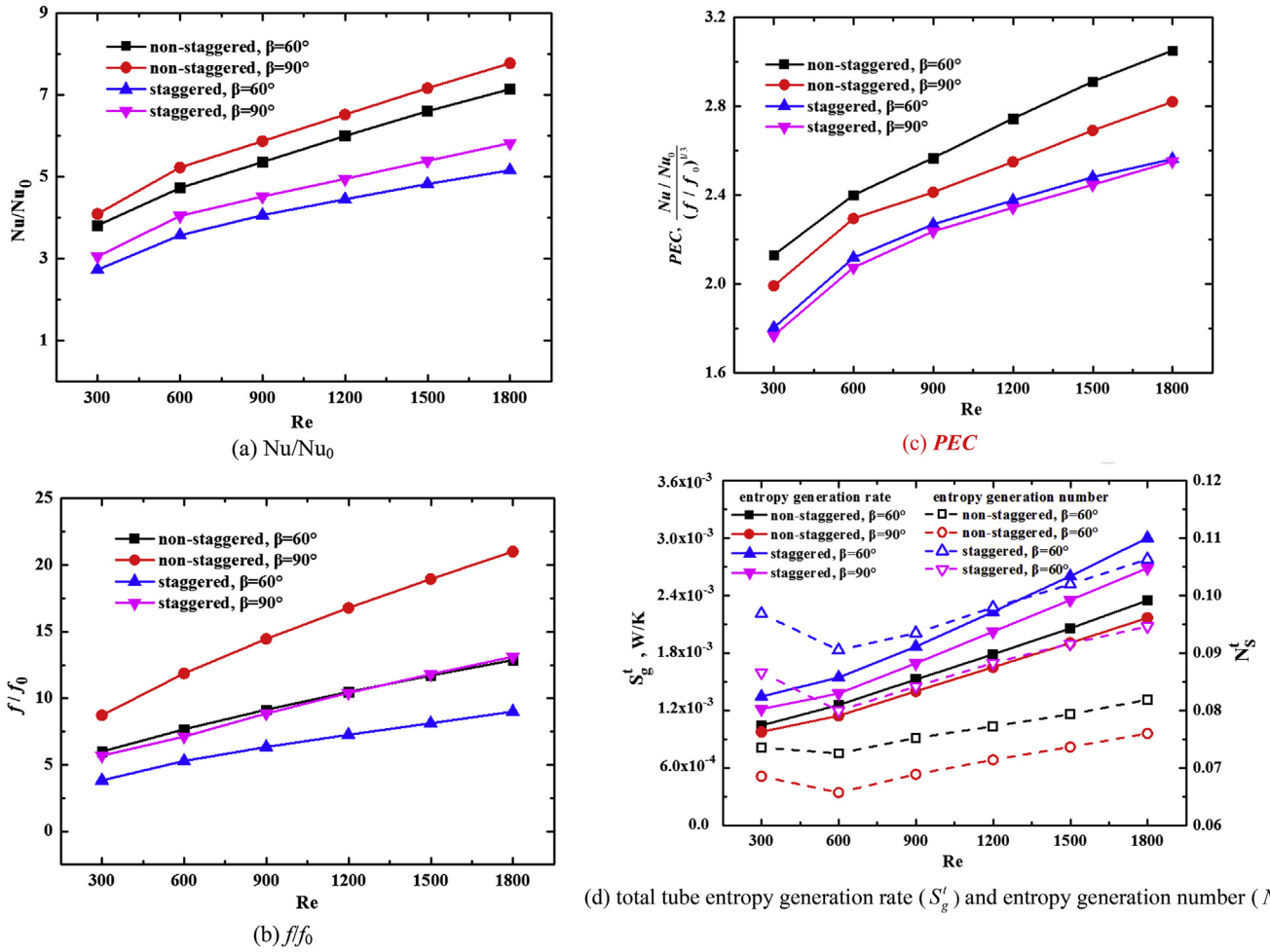

(a) Nu/Nu_0 (b) f/f_0 (c) *PEC* (d) total tube entropy generation rate (S_g^t) and entropy generation number (N_s^t)

Fig. 3. Comparisons of thermo-hydraulic performances for enhanced tubes with strip inserts of staggered and non-staggered alignments. The values of entropy generation rate and number in the curves are taken from enhanced tubes of 9*D* length. (a) Nu/Nu_0; (b) f/f_0; (c) PEC; (d) total tube entropy generation rate (S_g^t) and entropy generation number (N_s^t).

4. Results and discussions

4.1. Performance comparison between tubes with staggered and non-staggered strips

Two types of conical strips, i.e., geometry angle $\beta = 60^\circ$ and 90°, are adopted to compare the performances between tubes with strips of staggered and non-staggered alignments in the current investigation. Fig. 3(a) and (b) depicts the variations of Nusselt number ratio (Nu/Nu_0) and friction factor ratio (f/f_0) for the two alignments of strips in the laminar flow regime, respectively, in which the subscript 0 stands for the corresponding value of smooth tube. From Fig. 3(a) and (b), it can be seen that both Nu/Nu_0 and f/f_0 increase with the increment of Re. Moreover, compared with staggered strip inserts, the non-staggered alignment generates larger Nu/Nu_0 and f/f_0. In more details, the mean Nu/Nu_0 is about 35.6% and 31.9% higher for $\beta = 60^\circ$ and 90°, respectively, while the mean f/f_0 takes the values 46.2% and 60.9% larger than those of staggered alignment for the two geometry angles, respectively. The variation of overall thermo-hydraulic performance (PEC) is presented in Fig. 3(c). From Fig. 3(c) one can see that both non-staggered and staggered alignments of strips generate an increasing PEC with the increment of Re, and the PECs of the former are about 16.1% and 10.0% larger for $\beta = 60^\circ$ and 90°, respectively.

The comparisons of total entropy generation rate (S_g^t in left vertical axis) and entropy generation number (N_s^t in right vertical axis) between the staggered and non-staggered alignments are presented in Fig. 3(d), in which the entropy generations take the values of tubes with same length (i.e., 9D). From Fig. 3(d) it is clear that the irreversible losses of enhanced tubes with non-staggered strips are smaller than those of staggered alignment. In more details, S_g^t and N_s^t caused by non-staggered strips are about 81.1% and 80.0% of those by strips of staggered alignment, respectively.

In conclusion, the strips of non-staggered alignment could enhance the heat transfer rate more efficiently, because they generate relatively larger heat transfer rates and PECs, meanwhile the irreversible losses are smaller. Therefore, the following investigations in geometrical parameters are limited to the non-staggered strip inserts.

4.2. Variations of entropy generations with geometrical parameters

4.2.1. Effects of geometrical parameters on entropy generation rates resulting from heat transfer ($S_{g,\Delta T}^t$) and viscous flow ($S_{g,\Delta p}^t$)

Fig. 4(a)–(d) demonstrates the effects of slant angle (α), geometry angle (β), dimensionless strip-wall gap (δ/D) and strip pitch (b/D) on the entropy generation rates of enhanced tubes, respectively. Double vertical coordinates systems are adopted in Fig. 4, in which the left axis represents the entropy generation resulting from heat transfer ($S_{g,\Delta T}^t$), and right vertical axis stands for the viscous entropy generation ($S_{g,\Delta p}^t$). Both $S_{g,\Delta T}^t$ and $S_{g,\Delta p}^t$ take the values produced in the tubes of same length (i.e., 9D), and the

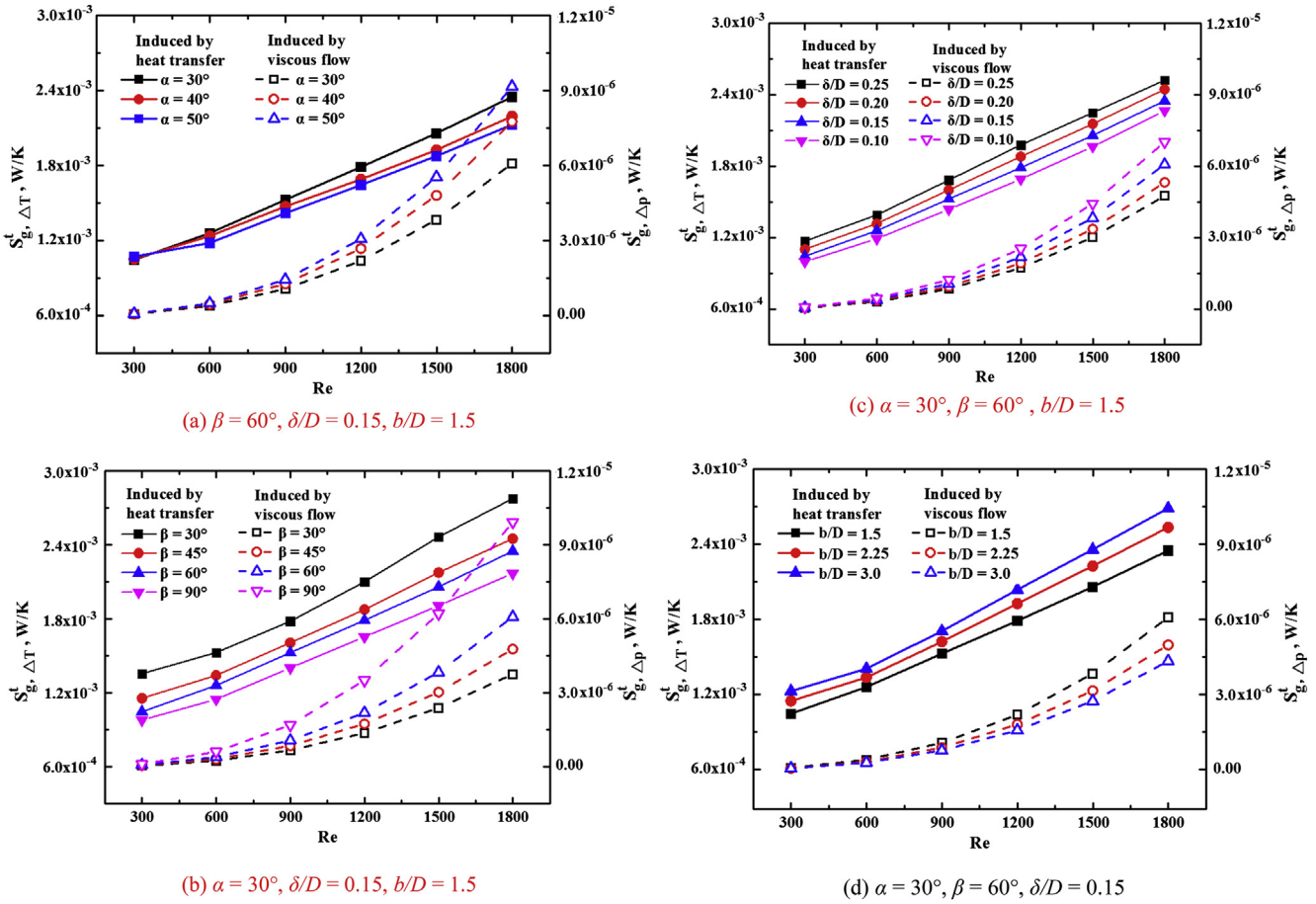

Fig. 4. Variations of tube entropy generation rate resulting from heat transfer ($S_{g,\Delta T}^t$) and viscous flow ($S_{g,\Delta p}^t$) for enhanced tubes with different slant angles (α), geometry angles (β), strip-wall gaps (δ/D) and strip pitches (b/D). The values of entropy generation rate in the curves are taken from enhanced tubes of 9D length. (a) $\beta = 60^\circ$, $\delta/D = 0.15$, $b/D = 1.5$; (b) $\alpha = 30^\circ$, $\delta/D = 0.15$, $b/D = 1.5$; (c) $\alpha = 30^\circ$, $\beta = 60^\circ$, $b/D = 1.5$; (d) $\alpha = 30^\circ$, $\beta = 60^\circ$, $\delta/D = 0.15$.

heat flux on tube wall varies between 400 and 800 W/m^2 for Re = 300–1800. It is clearly seen from Fig. 4(a)–(d) that the geometrical parameters exert significant effects on entropy generation rates, and two general tendencies are observed. First, both $S^t_{g,\Delta T}$ and $S^t_{g,\Delta p}$ increase with the increment of Re. Secondly, the values of $S^t_{g,\Delta T}$ are several hundred times larger than those of $S^t_{g,\Delta p}$. For an instance, when Re rises from 300 to 1800, the non-staggered strips of $\alpha = 30°$, $\beta = 60°$, $\delta/D = 0.15$ and $b/D = 1.5$ generate rising $S^t_{g,\Delta T}$ and $S^t_{g,\Delta p}$, and their values vary between 5.24E−4~1.18E−3 and 3.66E−8~3.04E−6 W/K, respectively, which indicate that the irreversible losses due to viscous flow could be neglected in the evaluation of total entropy generation, and thus $S^t_{g,\Delta T}$ is highlighted in the following analyses.

It is observed from Fig. 4(b)–(d) that at a fixed Re, $S^t_{g,\Delta p}$ increases with the increment of geometry angle (β), and with the decrements of strip-wall gap (δ/D) or pitch (b/D), while the variation tendencies of $S^t_{g,\Delta T}$ are inverse. In addition, as depicted in Fig. 4(a), $S^t_{g,\Delta p}$ increases with the increment of slant angle (α) monotonically. However, the variation tendency of $S^t_{g,\Delta T}$ versus α is more complex and depends on Re. When Re exceeds about 400, $S^t_{g,\Delta T}$ decreases with the increment of α; however, when Re = 300, $S^t_{g,\Delta T}$ increases with the increment of α, but the differences are not that large.

Scrutinizing the curves in Fig. 4(a)–(d), one can see that $S^t_{g,\Delta T}$ is most sensitive to the geometry angle (β). When β is increased from 30° to 90°, $S^t_{g,\Delta T}$ decreases by around 30.9%. The strip-wall gap (δ/D) and pitch (b/D) have moderate effects on the irreversible losses. The maximum averaged variations of $S^t_{g,\Delta T}$ caused by δ/D and b/D are about 15.6% and 13.9%, respectively (at $\delta/D = 0.1$ versus 0.25; $b/D = 1.5$ versus 3.0). The impact of slant angle (α) on the irreversible losses is relatively smaller with a maximum averaged variation of about 6.8%.

4.2.2. *Effects of geometrical parameters on the total entropy generation number (N^t_s)*

The total entropy generation rate (S^t_g) and dimensionless entropy generation number (N^t_s) are usually highlighted in the entropy generation analysis. Since the irreversible losses resulting from heat transfer are dominant in the total entropy generation, and the entropy generation rates of heat transfer have already been

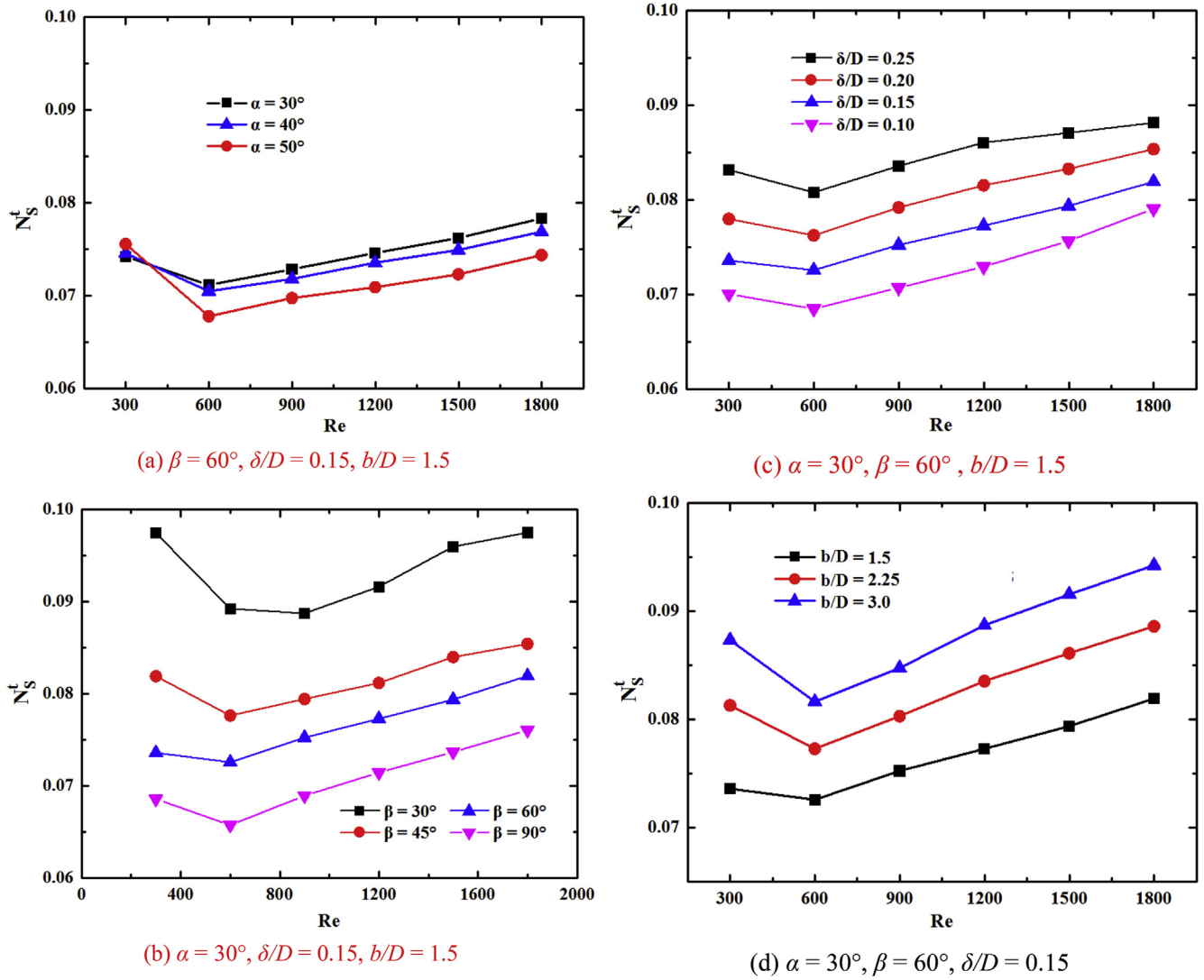

Fig. 5. Variation of total entropy generation number (N^t_s) for enhanced tubes with different slant angles (α), geometry angles (β), strip-wall gaps (δ/D) and strip pitches (b/D). The values of total entropy generation number in the curves are taken from enhanced tubes of 9D length. (a) $\beta = 60°$, $\delta/D = 0.15$, $b/D = 1.5$; (b) $\alpha = 30°$, $\delta/D = 0.15$, $b/D = 1.5$; (c) $\alpha = 30°$, $\beta = 60°$, $b/D = 1.5$; (d) $\alpha = 30°$, $\beta = 60°$, $\delta/D = 0.15$.

putted forward in Section 4.2.1, here only the variation of total entropy generation number is presented.

The influences of slant angle (α), geometry angle (β), strip-wall gap (δ/D) and strip pitch (b/D) on total entropy generation number (N_s^t) are presented in Fig. 5(a)–(d), respectively. From Fig. 5 it is seen that N_s^t lies in the range of 0.0657–0.0975 for all the investigated non-staggered strips and Re, and it has a different variation tendency with Re compared with $S_{g,\Delta T}^t$. All the curves of N_s^t–Re are concave and the pits are located at Re = 600. In other words, when Re < 600, N_s^t drops with an increasing Re, while a larger Re generates a larger N_s^t at Re > 600. This phenomenon indicates that the Re = 600 is an optimal working condition from the viewpoint of minimal entropy generation number.

Scrutinizing the curves in Fig. 5(a)–(d), one can see that geometry angle (β) has a larger influence on N_s^t. When β is increased from 30° to 90°, N_s^t decreases by around 32.2%. Meanwhile, the influences of strip-wall gap (δ/D) and pitch (b/D) are moderate with the maximum averaged relative variations about 16.5% and 14.8%, respectively (at δ/D = 0.1 versus 0.25; b/D = 1.5 versus 3.0). The impact of slant angle (α) on N_s^t is relatively limited. Its maximum averaged variation is about 6.9%.

4.3. Discussions and analyses

4.3.1. About the comparisons of thermo-hydraulic performances between staggered and non-staggered alignments

In Section 4.1, it is concluded that non-staggered strips generate larger heat transfer rates and smaller entropy generation rates compared with staggered ones. To dig the reason, the temperature and velocity contours at the longitudinal and cross sections of enhanced tubes with staggered or non-staggered strips are presented in Fig. 6(a)–(d), respectively. Comparing Fig. 6(c) and (d), one can see that the non-staggered alignment generates a larger velocity magnitude, which results in a larger pressure loss and viscous entropy generation rate, and also facilitates the enhancement of heat transfer rate and reduction of heat transfer entropy generation. Scrutinizing the velocity and temperature contours of the cross section in Fig. 6, one can find that compared with the insufficiently disturbed region of staggered alignment, where the local flow and thermal boundary layers are thicker, the counterpart of non-staggered alignment is smaller, which favors the increment of heat transfer rate and reduction of heat transfer entropy generation.

Studying the velocity contours in the longitudinal sections of Fig. 6(c) and (d), it is find that the velocity contour generated by staggered strips is more complicated, and the analysis on the comparison of heat transfer rate (and thus entropy generation by heat transfer) need to be based on the “field synergy principle”, which tells that the convection heat transfer rate depends on both fluid velocity magnitude and synergy angle between velocity and heat flux [43]. As for the tubes with staggered strips, due to the blockage of strips, the near-wall fluid has a smaller velocity magnitude at the downstream of strips, while there the synergy angle between velocity and heat flux is smaller, which facilitates a larger heat transfer rate. The fluid velocity on the opposite side of strips is larger, however, there the synergy performance between convection and heat conduction is not so desirable. As a result, the local convection heat transfer coefficient on the strip side has a

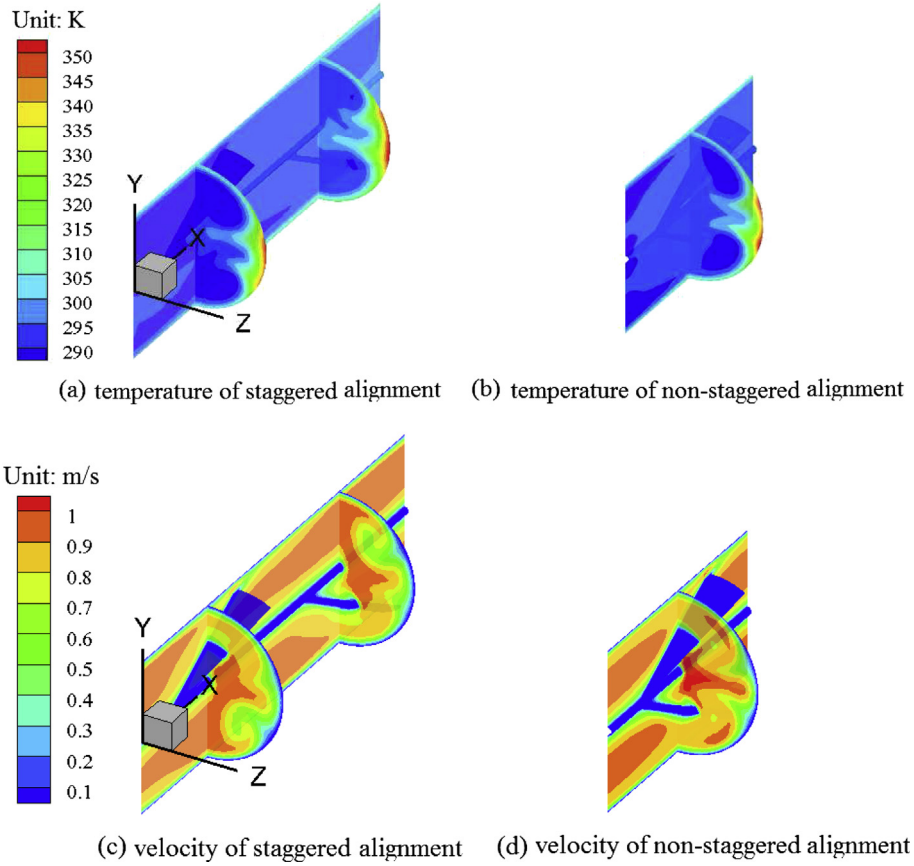

Fig. 6. Contours of temperature and velocity for enhanced tubes with strips of staggered and non-staggered alignments under the condition of Re = 900. (a) Temperature of staggered alignment; (b) temperature of non-staggered alignment; (c) velocity of staggered alignment; (d) velocity of non-staggered alignment.

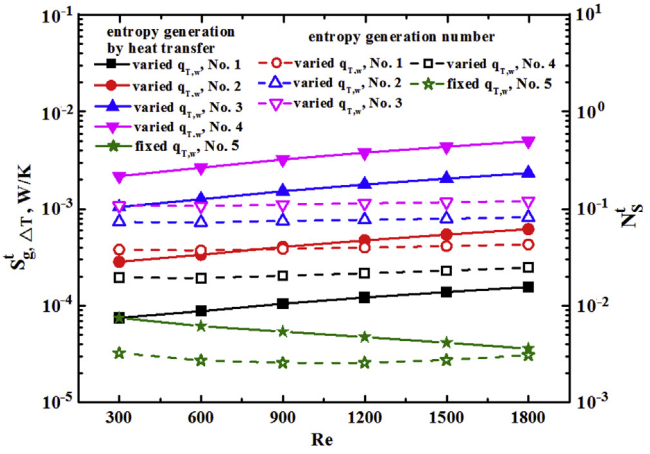

Fig. 7. Variations of tube entropy generation rate of heat transfer ($S^t_{g,\Delta T}$) and total entropy generation number (N^t_S) under five different heating conditions. The heat flux on tube wall is linear to Re for No. 1, 2, 3 and 4, and their values at Re = 300 are equal to 100, 200, 400 and 600 W/m^2, respectively. The tube wall of No. 5 has a constant heat flux of 100 W/m^2.

larger value, which can be seen from a thicker thermal boundary layer on the opposite side (see Fig. 6(a)). Non-staggered alignment accommodates two times strips compared with staggered one, which facilitates the heat transfer enhancement and also the reduction of heat transfer entropy generation.

With the above analyses, one can conclude that compared with staggered strips, non-staggered ones can generate good heat transfer enhancement, i.e., a larger Nu and a smaller entropy generation rate.

4.3.2. About the comparison of entropy generation rate of heat transfer ($S^t_{g,\Delta T}$) with that of viscous flow ($S^t_{g,\Delta p}$) and the effects of tube-wall heat flux ($q_{T,w}$)

Fig. 4 demonstrates that tube entropy generation rate resulting from heat transfer ($S^t_{g,\Delta T}$) overwhelms the counterpart caused by viscous flow ($S^t_{g,\Delta p}$). The reason for this phenomenon could lie in the adopted Re and tube-wall heat flux ($q_{T,w}$). On the one hand, the fluid velocity of present laminar flow is small, thus $S^t_{g,\Delta p}$ has a small value as well. On the other hand, a large $q_{T,w}$ (i.e., 400 W/m^2 at Re = 300) is adopted in the present investigation, and the temperature difference between tube wall and working fluid is large. Thus, a notable $S^t_{g,\Delta T}$ is generated and it plays a dominant role in the total entropy generation (S^t_g).

To further investigate the relation between heat flux ($q_{T,w}$) and entropy generation ($S^t_{g,\Delta T}$, $S^t_{g,\Delta p}$ and N^t_S), five different heating conditions are computed, among which four conditions have varied $q_{T,w}$ under different Re, while $q_{T,w}$ of the fifth condition is constant for all Re. The results are depicted in Fig. 7, where the left and right vertical axes are for $S^t_{g,\Delta T}$ and N^t_S, respectively. It is noted that because the value of $S^t_{g,\Delta p}$ is limited and the effects of $q_{T,w}$ on $S^t_{g,\Delta p}$ is relatively weak, no $S^t_{g,\Delta p}$–Re curves are showed in Fig. 7. Instead, the value of $S^t_{g,\Delta p}$ is referred to the black dashed curve in Fig. 4(a).

From the left vertical axis of Fig. 7, it is clearly seen that $S^t_{g,\Delta T}$ drops monotonically with a decreasing $q_{T,w}$ at a fixed Re. In more details, when Re = 900 and $q_{T,w}$ is decreased to one half or a quarter (i.e., from 560 to 280 or 140 W/m^2), $S^t_{g,\Delta T}$ will drop by about 73.4% and 93.1%, respectively. Compared with $S^t_{g,\Delta T}$, the total entropy generation number (N^t_S) has a more stable relation with $q_{T,w}$ (see the right vertical axis in Fig. 7). With the above variations of $q_{T,w}$, N^t_S drops to about 51.7% and 27.9%, respectively. In addition, Fig. 7 shows that the $S^t_{g,\Delta T}$–Re curves of varied heat flux are rising despite the heat transfer rate is larger at a larger Re. The variation trend can be reasoned as below:

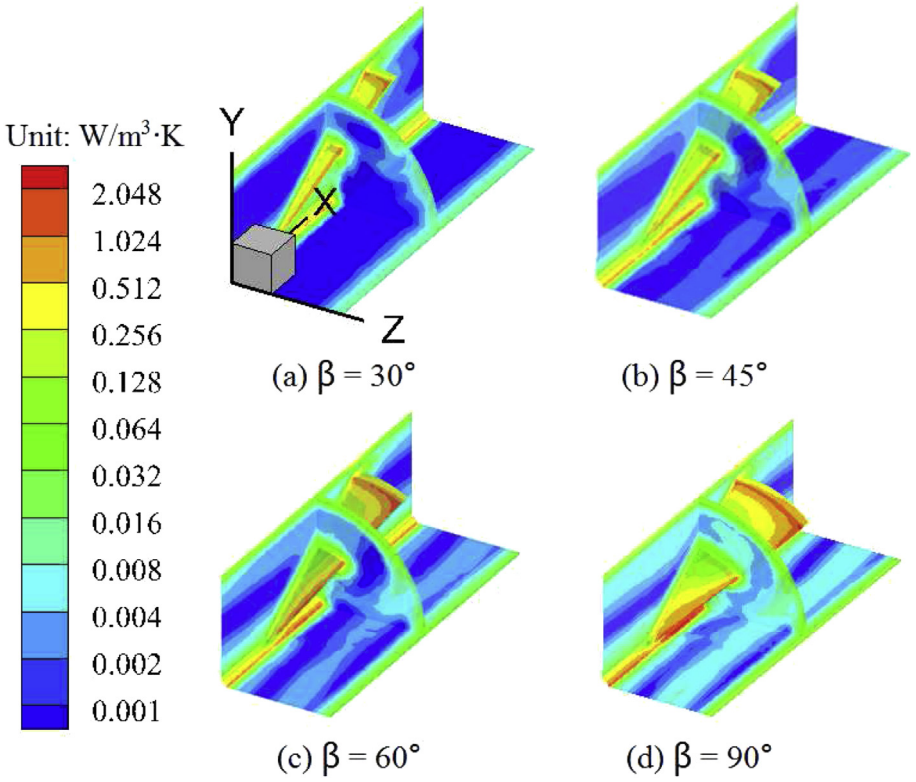

Fig. 8. Contours of local entropy generation rate induced by viscous flow ($S^e_{g,\Delta p}$) at horizontal, longitudinal planes and cross section for enhanced tubes with non-staggered strips of different geometry angles (β). (a) $\beta = 30°$; (b) $\beta = 45°$; (c) $\beta = 60°$; (d) $\beta = 90°$.

Under the conditions of varied heat flux of Fig. 7, tube-wall heat flux ($q_{T,w}$) is proportional to Re, and the slope is roughly the same as that of Nu (<1), thus the averaged fluid temperature is smaller at a larger Re, while the temperature differences between tube wall and working fluid at different Re are approximately the same. From the above two points, it is known that the tube-wall temperature decreases with a rising Re, while the entropy flow through tube wall rises with an increasing Re, which results in a larger entropy generation rate at a larger Re. The similar heating conditions are adopted in Fig. 4, and there $S^t_{g,\Delta T}$ increases with the increment of Re as well.

In addition, scrutinizing the curve of constant heat flux in Fig. 7 (marked with green (in the web version) stars), where $q_{T,w}$ has a low value of 100 W/m^2 for all investigated Re, one can see that different with the curves of $S^t_{g,\Delta T}$–Re under varied heat flux conditions in Figs. 4 and 7, $S^t_{g,\Delta T}$ of constant heat flux decreases with an increasing Re, dropping from about 7.5E−5 to 3.6E−5 W/K as Re rises from 300 to 1800. The variation tendency of $S^t_{g,\Delta p}$ with Re is monotonically increasing (refer to the black dashed curve in Fig. 4(a)), and its values at Re = 300 and 1800 are 7.58E−8 and 6.17E−6 W/K, respectively.

Compared with Ref. [26], where entropy generation of laminar heat transfer in curved duct was studied, the current study has qualitatively the same variation tendencies of $S^t_{g,\Delta T}$ and $S^t_{g,\Delta p}$ with Re under the condition of constant heat flux, as well as that of $S^t_{g,\Delta T}$ with heat flux. In addition, the De number ($De = S^t_{g,\Delta T}/S^t_{g,\Delta p}$) of current enhanced tube has a value about 5.8 under the condition of Re = 1800 and $q_{T,w}$ = 100 W/m^2, several times larger than but comparable to that reported in Ref. [26]. However, the temperature difference under such condition is limited (about 3 K).

4.3.3. About the variation tendency of entropy generation rate and number with geometrical parameters

As mentioned in Section 4.2.1 that tube entropy generation rate resulting from heat transfer ($S^t_{g,\Delta T}$) decreases with the increment of geometry angle (β), and with the decrements of strip-wall gap (δ/D) or strip pitch (b/D), while $S^t_{g,\Delta p}$ shows an opposite variation tendency (refer to Fig. 4). These variation trends could be explained by the Nu and f curves of enhanced tubes under various geometrical parameters depicted in Ref. [33], whose physical mechanisms were accounted for with the velocity and temperature contours at Re = 900 in the same paper. According to the Nu–Re and f–Re curves of Ref. [33] in which the dimensionless strip pitch is expressed with s/D, conical strip inserts with larger β, or smaller δ/D, or smaller b/D which is used to express strip pitch in the present paper, could give the fluid more intensive disturbances, and thus result in larger pressure losses and $S^t_{g,\Delta p}$. Meanwhile, the heat transfer rates are enhanced more effectively by such strips and the enhanced tubes have smaller heat transfer temperature differences (see Eq. (6)) at the same heat flux. As a result, the tube-wall temperature decreases and $S^t_{g,\Delta T}$ becomes relatively smaller. The irreversible loss of enhanced tubes resulting from viscous flow increases with slant angle (α), which could be interpreted by the f curves of Ref. [33]. However, as mentioned in Section 4.2.1, the heat transfer entropy generation increases with the increment of α when Re is larger than about 400, which can be interpreted by the Nu–Re curves and corresponding temperature contours under different α in Ref. [33]. When Re = 300, the entropy generation from heat transfer increases with the increment of α, this is in accordance with the decreasing relation between Nu and α in Ref. [33] as well.

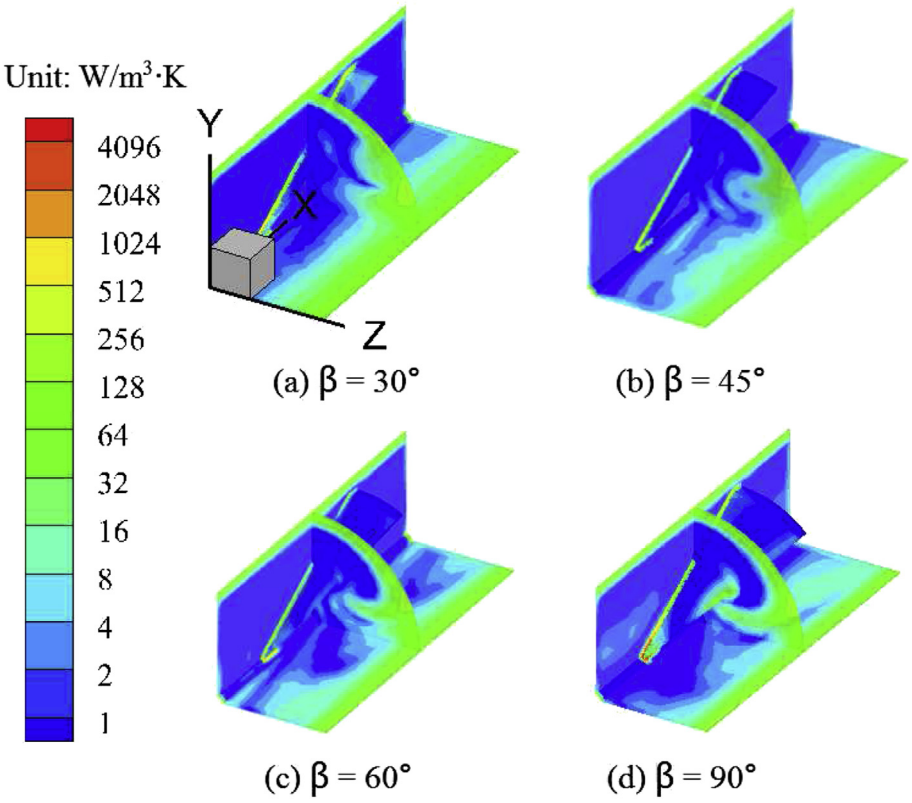

Fig. 9. Contours of local entropy generation rate induced by heat transfer ($S^c_{g,\Delta T}$) at horizontal, longitudinal planes and cross section for enhanced tubes with non-staggered strips of different geometry angles (β). (a) $\beta = 30°$; (b) $\beta = 45°$; (c) $\beta = 60°$; (d) $\beta = 90°$.

It is depicted in Fig. 5 that total entropy generation number N_s^t has a different variation tendency from that of entropy generation rate (S_g^t), i.e., it is concave with Re. It is known from the definition of N_s^t (Eq. (13)) that the above phenomenon is related to both the entropy generation rate and entropy flow of tube wall. On the one hand, it is known from Fig. 4 that entropy generation rate increases with the increment of Re. On the other hand, because the heat flux on tube wall is increased at approximately the same rate as that of Nu when Re is increased, the tube wall has a smaller temperature at a larger Re, therefore, the entropy flow through tube wall rises with an increasing Re. When Re is relatively smaller (i.e., Re < ~600), the variation of tube-wall entropy flow surpasses that of entropy generation rate, thus N_s^t drops with the increment of Re. However, for a relatively larger Re (i.e., Re > ~600), the increase of entropy generation rate with Re will exceed that of tube-wall entropy flow, thus the N_s^t rises with Re number.

4.3.4. Discussions based on local entropy generation rate

The above discussions are based on the analyses of augmentations of heat transfer rate and flow resistance, as well as the temperature and velocity contours of fluid. For further discussion, local entropy generation rates resulting from heat transfer and viscous flow (i.e., $S_{g,\Delta T}^c$ and $S_{g,\Delta p}^c$) of tubes with non-staggered strips are presented in Figs. 8 and 9, respectively, and corresponding contours of velocity magnitude and temperature are depicted in Figs. 10 and 11, respectively. It is noted that here only the impact of geometry angle (β) is discussed as an example.

From Fig. 8(a)–(d), it is seen that $S_{g,\Delta p}^c$ is relatively larger in the near-wall regions for all cases, especially in the very vicinity of the walls of strip and rod. The reason is that the velocity gradient (and thus strain rate) in those regions is relatively larger (see Fig. 10(a)–(d)), and local viscous heating or irreversible loss of mechanical work is more notable. In addition, since Re remains constant in Fig. 8, the fluid velocity magnitude increases with the increment of β (see Fig. 10), thus, a larger β facilitates a larger $S_{g,\Delta p}^c$. Meanwhile, a larger β indicates that a strip has a larger strip-wall surface, near which $S_{g,\Delta p}^c$ has a larger value (refer to Fig. 8). Due to the above two points, $S_{g,\Delta p}^t$ increases with the increment of β, which is in accordance with Fig. 4(b).

Similar to the distribution of $S_{g,\Delta p}^c$, $S_{g,\Delta T}^c$ is mainly located in the region near tube wall, and it has much larger values than $S_{g,\Delta p}^c$(refer to Fig. 9). The reason is that the present heat transfer temperature difference between tube wall and working fluid, mainly in the region near tube wall, is 20–30 times that of fluid velocity. Moreover, it is seen from Fig. 9 that the horizontal section ($Y = 0$) has a considerably thick layer of larger $S_{g,\Delta T}^c$ next to tube wall. This local distribution of $S_{g,\Delta T}^c$ could explained as following:

The horizontal section ($Y = 0$) is far away the installation plane of strips, and there the disturbance is relatively weaker compared with the longitudinal section (see Fig. 10). Therefore, the horizontal section has a larger tube-wall temperature and thicker thermal boundary layer (see Fig. 11), which generate a considerable $S_{g,\Delta T}^c$.

Comparing $S_{g,\Delta p}^c$ and $S_{g,\Delta T}^c$ with the counterparts in Ref. [26], it is clear that both ducts have the majority of entropy generation in the near-wall region. Moreover, the current $S_{g,\Delta p}^c$ is several times larger than that in Ref. [26], while $S_{g,\Delta T}^c$ is even dozens or hundreds times larger. The former can be reasoned by the larger increment of friction loss resulting from strips, while the reason to the latter can

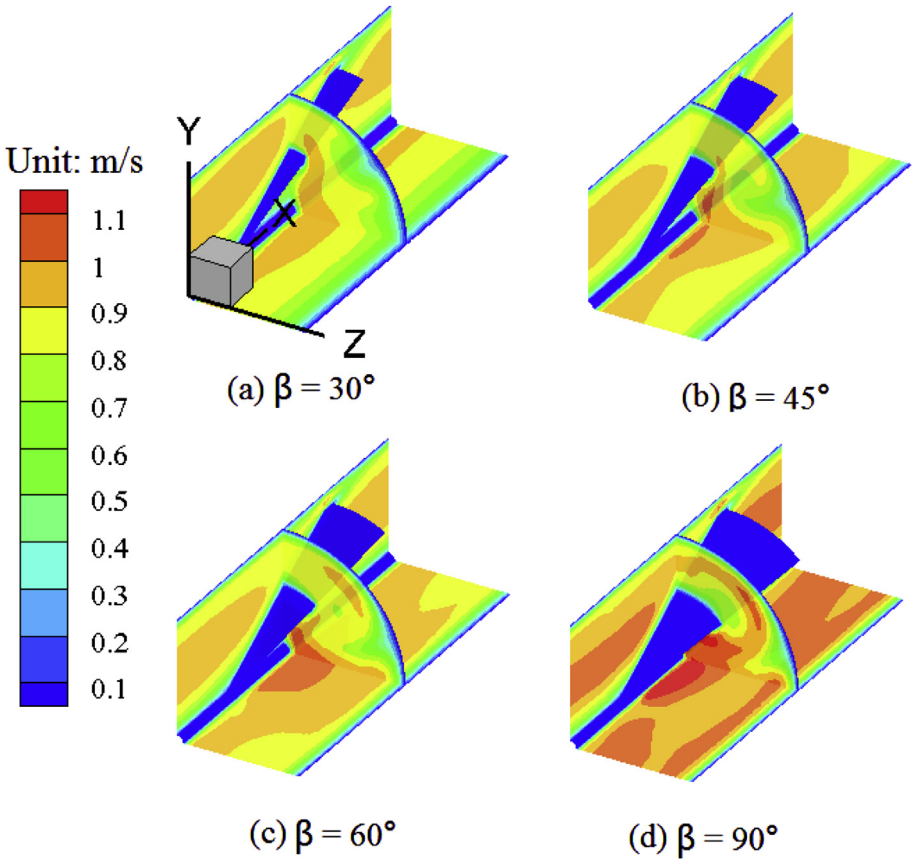

Fig. 10. Contours of velocity magnitude at horizontal, longitudinal planes and cross section for enhanced tubes with non-staggered strips of different geometry angles (β). (a) $\beta = 30°$; (b) $\beta = 45°$; (c) $\beta = 60°$; (d) $\beta = 90°$.

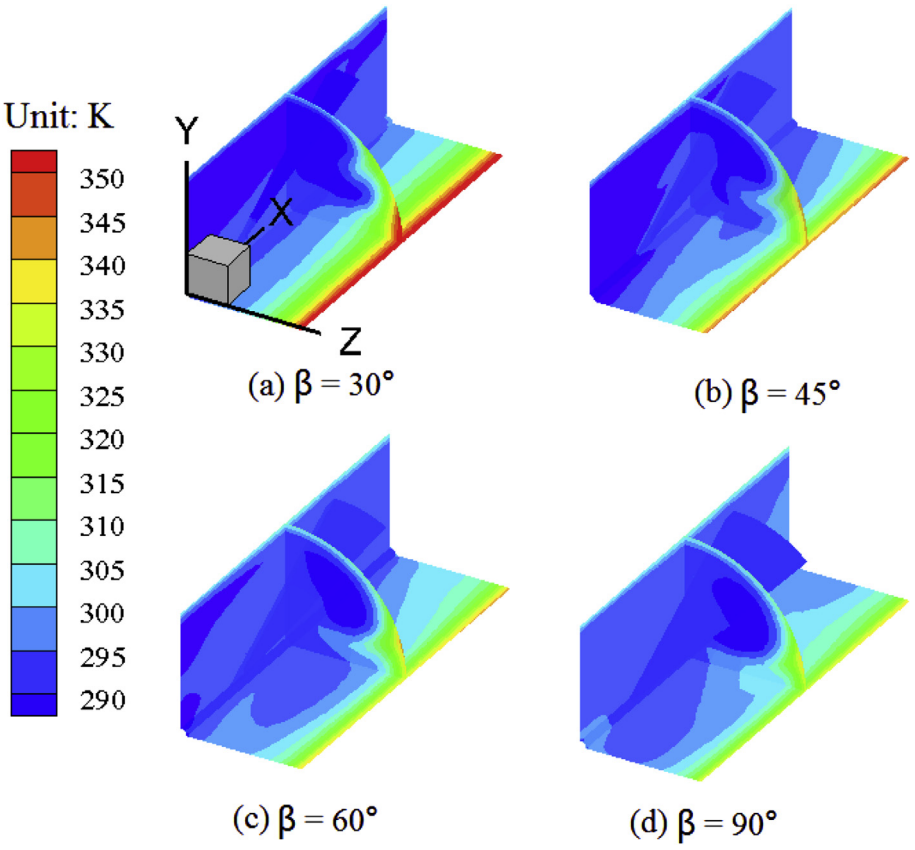

Fig. 11. Contours of temperature at horizontal, longitudinal planes and cross section for enhanced tubes with non-staggered strips of different geometry angles (β). (a) $\beta = 30°$; (b) $\beta = 45°$; (c) $\beta = 60°$; (d) $\beta = 90°$.

be the larger heat flux adopted in the current investigation, which can be seen by comparing the $S^c_{g,\Delta T}$ of the thin layer near heated wall.

In addition, the comparisons of local entropy generation rates between non-staggered alignments (see Figs. 8 and 9) and staggered ones (see Figs. 12 and 13) are conducted. From the comparisons, one can see that the non-staggered alignment results in a smaller $S^c_{g,\Delta T}$, while the $S^c_{g,\Delta p}$ of staggered alignment is smaller. The reason is that non-staggered strips could enhance heat transfer rate more effectively, while staggered strips generate smaller flow

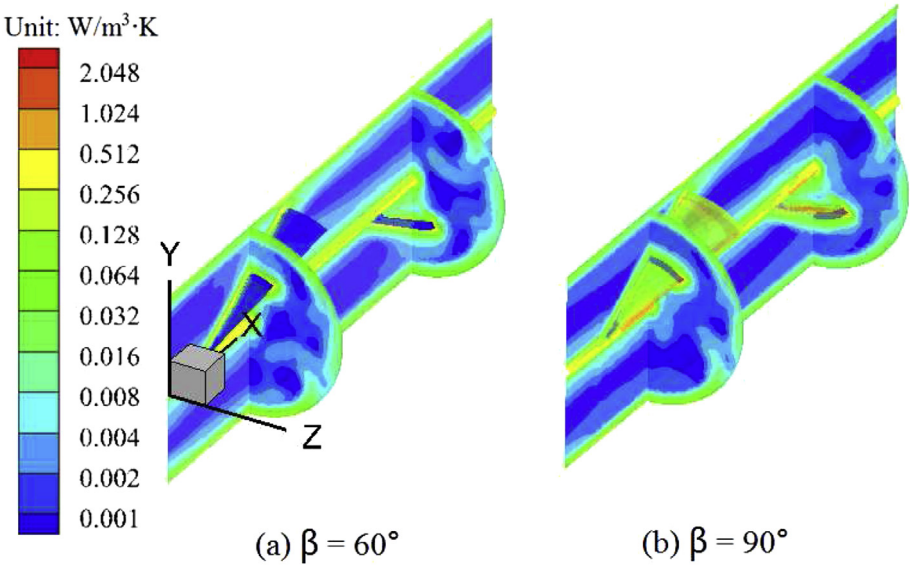

Fig. 12. Contours of local entropy generation rate induced by viscous flow ($S^c_{g,\Delta p}$) at longitudinal plane and cross sections for enhanced tubes with staggered strips of different geometry angles (β). (a) $\beta = 60°$; (b) $\beta = 90°$.

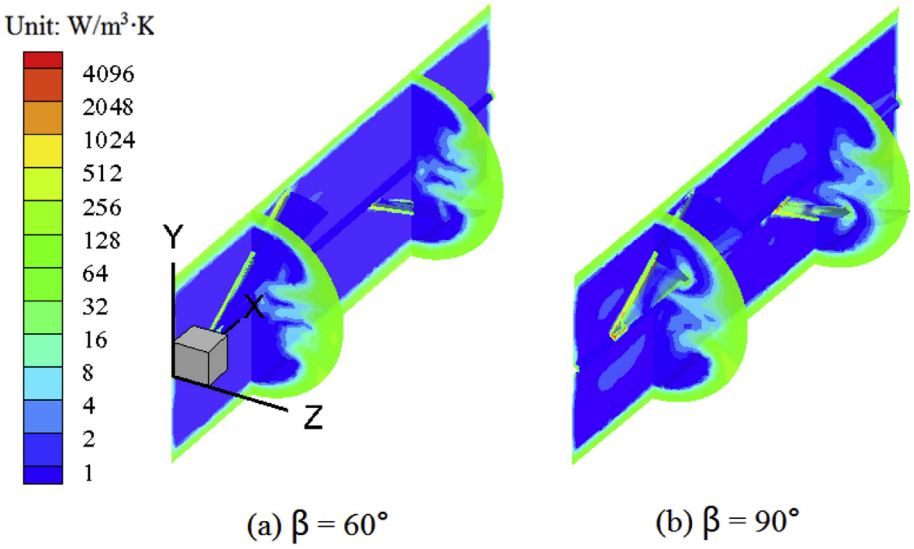

Fig. 13. Contours of local entropy generation rate induced by heat transfer ($S^{t}_{g,\Delta T}$) at longitudinal plane and cross sections for enhanced tubes with staggered strips of different geometry angles (β). (a) $\beta = 60°$; (b) $\beta = 90°$.

resistances (refer to Fig. 3(a) and (b), respectively), in accordance with the curves in Fig. 3(d).

5. Conclusions

The current work investigated the laminar thermal augmentation of horizontal circular tubes with conical strip inserts from the viewpoint of minimal entropy generation, including comparing thermo-hydraulic performances of enhanced tubes with staggered and non-staggered strip inserts, and examining the effects of geometrical parameters of strip inserts on the irreversible losses. Besides, the local entropy generations are presented for discussions and analyses. From the current study, some conclusions are obtained as below:

(1) The tubes with non-staggered strips behave better than those with staggered ones. The tube entropy generation rates of the former are about 81.1% of the latter, while their heat transfer rates and PECs are about 33.8% and 13.5% larger than the latter.
(2) Tube entropy generation rates resulting from heat transfer ($S^{t}_{g,\Delta T}$) and viscous flow ($S^{t}_{g,\Delta p}$) both increase with the increment of Re number. $S^{t}_{g,\Delta T}$ decreases with the increment of geometry angle, and with the decrements of dimensionless strip-wall gap or strip pitch, while the variation tendency of $S^{t}_{g,\Delta p}$ with the three parameters is opposite. In addition, the values of $S^{t}_{g,\Delta T}$ overwhelm those of $S^{t}_{g,\Delta p}$ under the current investigation conditions.
(3) The total entropy generation number (N^{t}_{s}), ranging between 0.0657 and 0.0975, has a variation trend of concave curve with Re, and the Re at the pit is about 600. N^{t}_{s} is most sensitive to geometry angle (β) with the maximum averaged relative variation about 32.2%. The strip-wall gap (δ/D) and strip pitch (b/D) have moderate impacts on N^{t}_{s} with the maximum averaged variations about 16.5% and 14.8%, respectively.

In brief, as for all the investigated enhanced tubes, the non-staggered strip insert with geometry angle $\beta = 90°$, strip-wall gap $\delta/D = 0.15$ and strip pitch $b/D = 1.5$ results in the least entropy generation rate and entropy generation number. In addition, the total entropy generation number of enhanced tube is minimal at the Re = 600 in the current investigation.

Acknowledgments

This work was supported by the National Key Basic Research Development Program of China (No. 2013CB228302) and the National Natural Science Foundation of China (No. 51036003).

References

[1] K.J. Bell, Heat exchanger design for the process industries, J. Heat Transf. 126 (2004) 877–885.
[2] R. Mukherjee, Effectively design shell-and-tube heat exchanger, Chem. Eng. Prog. 94 (2) (1998) 21–37.
[3] V.V. Wadekar, P. Sthlik, Different strategies to improve industrial heat exchanger, Heat Transf. Eng. 23 (6) (2002) 36–48.
[4] C.C. Gentry, Rodbaffle heat exchanger technology, Chem. Eng. Prog. 86 (7) (1990) 48–57.
[5] J. Lutcha, J. Nemcansky, Performance improvement of tubular heat exchangers by helical baffles, Chem. Eng. Res. Des. 68 (3) (1990) 263–270.
[6] Y.H. You, A.W. Fan, X.J. Lai, W. Liu, S.Y. Huang, Experimental and numerical study of thermal-hydraulic performance of a shell-and-tube heat exchanger with trefoil-hole baffles, Appl. Therm. Eng. 50 (1) (2013) 950–956.
[7] Y.H. You, A.W. Fan, S.Y. Huang, W. Liu, Numerical modeling and experimental validation of heat transfer and flow resistance on the shell side of a shell-and-tube heat exchanger with flower baffles, Int. J. Heat Mass Transf. 25–26 (55) (2012) 7561–7569.
[8] A.W. Fan, J.J. Deng, A. Nakayama, W. Liu, Parametric study on turbulent heat transfer and flow characteristics in a circular tube fitted with louvered strip inserts, Int. J. Heat Mass Transf. 55 (2012) 5205–5213.
[9] S. Ganeshan, M.R. Rao, Studies on thermo-hydraulics of single- and multi-start spirally corrugated tubes for water and time-independent power law fluids, Int. J. Heat Mass Transf. 25 (1982) 1013–1022.
[10] D.L. Gee, R.L. Webb, Forced convection heat transfer in helically rib-roughened tubes, Int. J. Heat Mass Transf. 23 (1980) 1127–1136.
[11] S.J. Eckels, T.M. Doerr, M.B. Pate, Heat transfer and pressure drop of r-134a and ester lubricant mixtures in a smooth and a micro-fin tube: part I – evaporation, ASHRAE Trans. 100 (2) (1994) 265–281.
[12] P. Naphon, Heat transfer and pressure drop in the horizontal double pipes with and without twisted tape insert, Int. Commun. Heat Mass Transf. 33 (2006) 166–175.
[13] R.M. Manglik, A.E. Bergles, Heat transfer and pressure drop correlations for twisted tape inserts in isothermal tubes: part I – laminar flows, J. Heat Transf. 115 (1993) 881–889.
[14] S.K. Saha, A. Dutta, S.K. Dhal, Friction and heat transfer characteristics of laminar swirl flow through a circular tube fitted with regularly spaced twisted-tape elements, Int. J. Heat Mass Transf. 44 (2001) 4211–4223.
[15] S. Eiamsa-ard, C. Thianpong, P. Promvonge, Experimental investigation of heat transfer and flow friction in a circular tube fitted with regularly spaced

twisted tape elements, Int. Commun. Heat Mass Transf. 33 (2006) 1225–1233.
[16] S.W. Chang, T.L. Yang, J.S. Liou, Heat transfer and pressure drop in tube with broken twisted tape insert, Exp. Therm. Fluid Sci. 32 (2007) 489–501.
[17] J. Guo, A.W. Fan, X.Y. Zhang, W. Liu, A numerical study on heat transfer and friction factor characteristics of laminar flow in a circular tube fitted with center-cleared twisted tape, Int. J. Therm. Sci. 50 (2011) 1263–1270.
[18] M.R. Rethu, M.R. Rao, Turbulent flow heat transfer and fluid friction in helical wire coil inserted tubes, Int. J. Heat Mass Transf. 26 (1) (1983) 1833–1845.
[19] A. Garcia, P.G. Vicente, Experimental study of heat transfer enhancement with wire coil inserts in laminar–transition–turbulent regimes at different numbers, Int. J. Heat Mass Transf. 48 (2005) 4640–4651.
[20] R.L. Webb, Performance evaluation criteria for use of enhanced heat transfer surfaces in heat exchanger design, Int. J. Heat Mass Transf. 24 (1981) 715–726.
[21] A. Bejan, Entropy Generation through Heat and Fluid Flow, Wiley, New York, 1982.
[22] A. Bejan, Entropy Generation Minimization, CRC Press, Boca Raton, FL, 1996.
[23] A. Bejan, Method of entropy generation minimization, or modeling and optimization based on combined heat transfer and thermodynamics, Rev. Gen. Therm. 35 (1996) 637–646.
[24] A.Z. Sahin, Irreversibilities in various duct geometries with constant wall heat flux and laminar flow, Energy 23 (6) (1998) 465–473.
[25] A.Z. Sahin, Thermodynamics of laminar viscous flow through a duct subjected to constant heat flux, Energy 21 (12) (1996) 1179–1187.
[26] T.H. Ko, K. Ting, Entropy generation and optimal analysis for laminar forced convection in curved rectangular ducts: a numerical study, Int. J. Therm. Sci. 45 (2) (2006) 138–150.
[27] T.H. Ko, A numerical study on entropy generation and optimization for laminar forced convection in a rectangular curved duct with longitudinal ribs, Int. J. Therm. Sci. 45 (2006) 1113–1125.
[28] P.K. Nag, K. Naresh, Second law optimization of convection heat transfer through a duct with constant heat flux, Int. J. Energy Res. 13 (1989) 537–543.
[29] H. Shokouhmand, M.R. Salimpour, Optimal Reynolds number of laminar forced convection in a helical tube subjected to uniform wall temperature, Int. Commun. Heat Mass Transf. 34 (2007) 753–761.
[30] T.H. Ko, A numerical study on developing laminar forced convection and entropy generation in half- and double-sine ducts, Int. J. Therm. Sci. 46 (2007) 1275–1284.
[31] A.Z. Sahin, Second law analysis of laminar viscous flow through a duct subjected to constant wall temperature, J. Heat Transf. 120 (1998) 76–83.
[32] A.W. Fan, J.J. Deng, J. Guo, W. Liu, A numerical study on thermo-hydraulic characteristics of turbulent flow in a circular tube fitted with conical strip inserts, Appl. Therm. Eng. 31 (2011) 2819–2828.
[33] Y.H. You, A.W. Fan, W. Liu, S.Y. Huang, Thermo-hydraulic characteristics of laminar flow in an enhanced tube with conical strip inserts, Int. J. Therm. Sci. 61 (2012) 28–37.
[34] J.P. Holman, Heat Transfer, McGraw-Hill, New York, 1997.
[35] A. Ebrahimi, S. Kheradmand, Numerical simulation of performance augmentation in a plate fin heat exchanger using winglet type vortex generators, Int. J. Mech. Eng. Mechatron. ISSN: 1929-2724 1 (1) (2012).
[36] Y.L. He, H. Han, W.Q. Tao, Y.W. Zhang, Numerical study of heat transfer enhancement by punched winglet-type vortex generator arrays in fin-and-tube heat exchangers, Int. J. Heat Mass Transf. 21–22 (55) (2012) 5449–5458.
[37] W.Q. Tao, Numerical Heat Transfer, second ed., Xi'an Jiaotong University Press, Xi'an, 2001 (in Chinese).
[38] ANSYS Fluent 12 Theory Guide, ANSYS Inc., USA, 2009.
[39] R.E. Sonntag, C. Borgnakke, Introduction to Engineering Thermodynamics, Wiley, New York, 2001.
[40] A.L. London, R.K. Shah, Costs of irreversibilities in heat exchanger design, Heat Transf. Eng. 4 (1983) 59–73.
[41] J.E. Hesselgreaves, Rationalisation of second law analysis of heat exchangers, Int. J. Heat Mass Transf. 43 (2000) 4189–4204.
[42] Z.W. Ni, Z.L. Jiao, Computation of the entropy increase and its total rate in heat exchanger, J. Eng. Thermophys. 9 (1988) 4–6 (in Chinese).
[43] W.Q. Tao, Z.Y. Guo, B.X. Wang, Field synergy principle for enhancing convective heat transfer – its extension and numerical verification, Int. J. Heat Mass Transf. 45 (2002) 3849–3856.